JOURNAL OF PROPULSION AND POWER
Vol. 20, No. 2, March–April 2004

Mach 4 Performance of Hypersonic Inlet with Rectangular-to-Elliptical Shape Transition

Michael K. Smart* and Carl A. Trexler†
NASA Langley Research Center, Hampton, Virginia 23681

Wind-tunnel testing of a hypersonic inlet with rectangular-to-elliptical shape transition has been conducted at Mach 4.0. This fixed geometry inlet had a geometric contraction ratio of 4.8 and was designed using a quasi-streamline tracing technique to have a design point of Mach 5.7. These tests were performed to investigate the starting and backpressure limits of the inlet at conditions well below its design point. Results showed that the inlet required side spillage holes in order to self-start at Mach 4.0. Once started, the inlet generated a compression ratio of 12.6, captured almost 80% of available air and withstood a backpressure ratio of 30.3 relative to tunnel static pressure. The spillage penalty for self-starting was estimated to be 3.4% of available air. These experimental results, along with previous experimental results at Mach 6.2, indicate that fixed-geometry inlets with rectangular-to-elliptical shape transition are a viable configuration for airframe-integrated scramjets that operate over a significant Mach-number range.

Nomenclature

A_{cap}	=	100% frontal area of the inlet; 4.55 in.^{2}
A_{fm}	=	flow meter throat area
C_D	=	discharge coefficient for flowmeter; 0.999 ± 0.002
D_h	=	hydraulic diameter of the elliptical isolator; 1.041 in.
L_{isol}	=	isolator length
M	=	Mach number
m_c	=	mass capture ratio; $\dot{m}_{\text{cap}}/\dot{m}_{100\%}$
$\dot{m}_{\text{cap}}$	=	airflow rate captured by the inlet
$\dot{m}_{100\%}$	=	freestream airflow rate through A_{cap}
p	=	pressure
u	=	velocity
x	=	model streamwise coordinate
γ	=	ratio of specific heats; 1.40 for air
ρ	=	density

Subscripts

close	=	inlet closure
ex	=	inlet exit
in	=	inside
max	=	maximum backpressure
out	=	outside
$t2$	=	Pitot
uns	=	unstart
1	=	wind-tunnel freestream
3	=	station in flowmeter used for mass flow calculation

Introduction

THE design of inlets for hypersonic vehicles utilizing airframe-integrated scramjet modules is a subject of interest in the high-speed propulsion community. In these configurations the vehicle bow shock performs the initial compression, and the capture shape of each scramjet module is required to be rectangular. Other requirements are that inlets will start at ramjet takeover speeds, operate over a large Mach number range, and be efficient during vehicle cruise. There is also a strong desire to have an intake with both fixed geometry and no requirement for boundary-layer bleed, in order to reduce the overall mechanical complexity of the system. Another beneficial feature of a hypersonic inlet for some scramjet applications is a transition from a rectangular capture to an elliptical throat. The inlet can then be used in combination with an elliptical combustor, which is superior to a rectangular combustor in terms of the structural weight required to withstand a specified pressure/thermal load and the wetted surface area needed to enclose a specified cross-sectional area. This type of configuration also reduces undesirable effects associated with hypersonic corner flows.

A number of three-dimensionally curved inlets leading to circular or elliptical combustors were designed and tested in the 1960s.[1–4] These fixed-geometry inlets performed well during wind-tunnel tests and self-started with internal contraction ratios considerably above the one-dimensional theoretical starting limit first introduced by Kantrowitz and Donaldson.[5] Some recent work on three-dimensionally curved inlets has utilized streamline-tracing techniques to design high-performance inlet configurations that include a transition from a nearly rectangular capture to an elliptical throat. A detailed methodology for the design of these fixed-geometry, rectangular-to-elliptical shape transition (REST) inlets was reported in Ref. 6. A description of the Mach 6.2 testing of a REST inlet with a design point of Mach 6.0 was reported in Ref. 7. The results of some computational analysis of these experiments was reported in Ref. 8.

Streamline-tracing techniques are a commonly used method for the design of three-dimensionally curved inlets. These techniques utilize an existing compressive flowfield and a chosen capture shape to construct an inviscid inlet surface from the flowfield streamlines that pass through the perimeter of the capture shape. Streamline-traced inlets therefore have an inherent design point or design Mach number that is dictated by the original flowfield used to generate the inlet. The procedure is completed by making allowance for local boundary-layer displacement thickness on the inlet surface. Operation of a well-designed streamline-traced inlet at its design point will nearly recreate the original internal flowfield. In this instance the inlet performance will be identical to the original flowfield, except for viscous losses at the walls and associated interactions. For scramjet applications, the design Mach number of a streamline-traced inlet is usually chosen to be close to the maximum operational Mach number to avoid oversped conditions.

The REST inlet design procedure[6] is a quasi-streamline-tracing technique that makes use of multiple sets of streamlines to perform

Presented as Paper 2003-0012 at the 41st Aerospace Sciences Meeting, Reno, NV, 6–9 January 2003; received 18 March 2003; revision received 21 August 2003; accepted for publication 21 August 2003.

*Aerospace Engineer, Hypersonic Airbreathing Propulsion Branch, MS 168. Senior Member AIAA.
†Aerospace Engineer, Hypersonic Airbreathing Propulsion Branch, MS 168.

the required transition from a rectangular capture to an elliptical throat. The suitability of this procedure for the design of a Mach 6 scramjet inlet operating at conditions close to the design point has been experimentally verified.[7] A key requirement for scramjet inlets is the ability to start at ramjet takeover speed (Mach 3–4). As the design point of a REST scramjet inlet will be well above this speed, an operational REST inlet must self-start and provide adequate compression at Mach numbers considerably below the design point.

This paper describes an experimental investigation of the off-design performance of REST inlets. These tests were performed at Mach 4.0 and involved a REST inlet with a design point of Mach 5.7. The goal of these experiments was to determine the starting characteristics and compressive performance of a REST inlet when operating at speeds well below the design point.

Experimental Program

Wind-Tunnel Test Conditions and Instrumentation

The experiments were conducted at NASA Langley Research Center in the Mach 4 Blown Down Facility (M4BDF). Typical operating conditions were a Mach number of 4.03, a stagnation pressure of 200 psia (1.38 Mpa), a stagnation temperature of 522° R (290 K), and a Reynolds number of 20×10^6/ft (6.1×10^6/m). The M4BDF has a 9×9 in. (22.9×22.9 cm) test section, which is 3 ft (0.91m) in length. Diagnostic instrumentation for the tests included 41 surface pressure taps, an eight-probe pitot rake at the exit of the inlet, a thermocouple to monitor the model temperature, and a Schlieren system for visualization of the external flow. The mass flow rate through the inlet was determined using a sonic throat-based flow-metering device. Model pressures were measured using a Pressure Systems, Inc., Model 780 electronically scanning pressure system. Two pressure ranges were utilized in the tests: 0–30 psia (0–204 kPa) and 0–75 psia (0–517 kPa). The error associated with the use of these transducers was ±0.5% full scale. The type J thermocouple used to monitor model temperature was of beaded construction and had an error of ±0.75% of the temperature measured above the 273 K reference. All facility and model data were acquired and saved using a PC-based data-acquisition system, and typical runs lasted approximately 2 min.

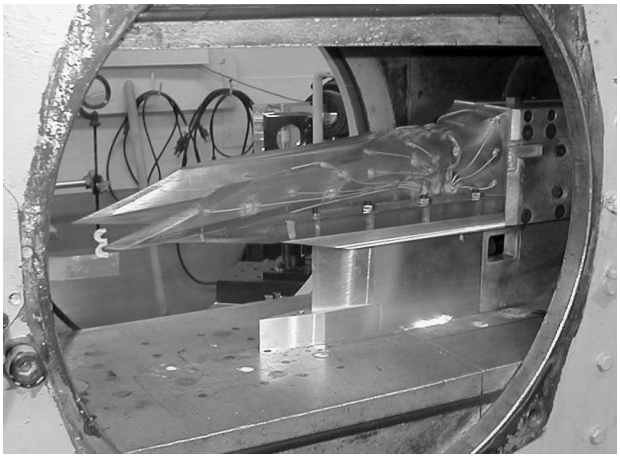

Fig. 1 REST inlet installed in the M4BDF.

Inlet Model

Figure 1 shows a photograph of the inlet installed in the wind-tunnel test section. The model was manufactured at NASA Langley using a stereolithography technique. This method enabled the three-dimensional internal inlet shape to be manufactured for approximately 1/10th of the cost of an aluminum model. The epoxy model produced with this technique had 0.025-in.-radius leading edges and was able to withstand conditions in the M4BDF test section with the addition of fiberglass reinforcement on the external cowl surface.

Three views of the inlet model are shown in Fig. 2. The model had a total length of 14.44 in., with cowl closure 8.95 in. from its most forward point, and the throat 12.52 in. from its most forward point. The model included a 1.75-in.-long elliptical isolator downstream of the throat, which corresponded to a $L_{\text{isol}}/D_h = 1.68$. The capture area of 4.55 in.^{2} was 3.0 in. wide, and the 100% capture mass flow rate for the inlet was $\dot{m}_{100\%} = 1.92$ lb/s. The inlet throat area was 0.947 in.^{2}, leading to a geometric contraction ratio of 4.80.

Figure 3 shows a schematic of the nominal streamlines along which surface pressure taps were distributed. Internal pressure taps were concentrated on one side of the model (as the model had a vertical plane of symmetry) and were placed on the six streamlines (labeled A, C, D, E, G, and H in Fig. 3) at eight different axial stations along the inlet. Two extra taps were added at the exit (B and F in Fig. 3), and a solitary external pressure tap was included just downstream of cowl closure in order to monitor inlet spillage

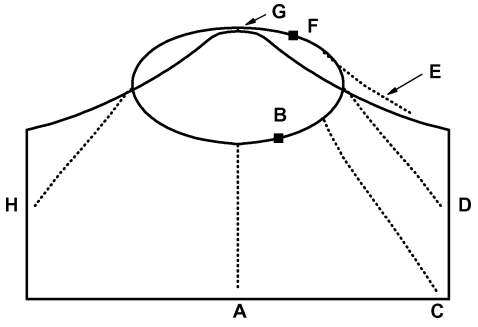

Fig. 3 Schematic of the instrumentation streamlines.

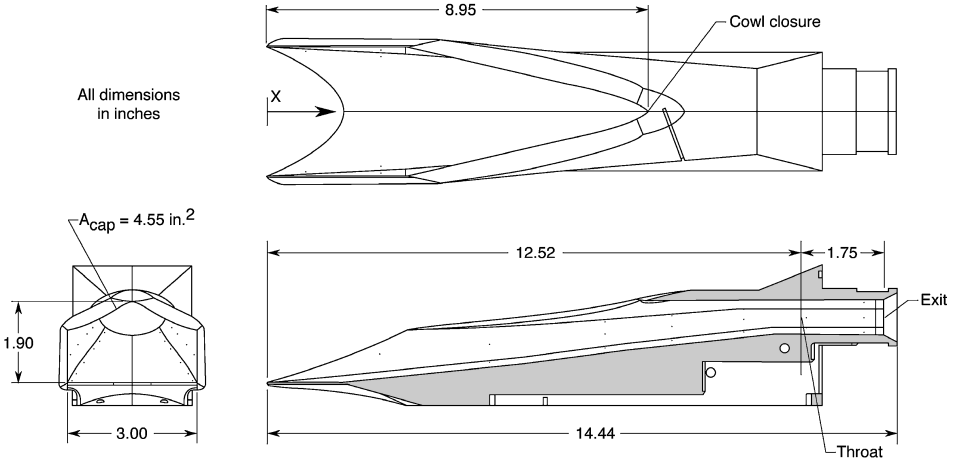

Fig. 2 Three views of the REST inlet model.

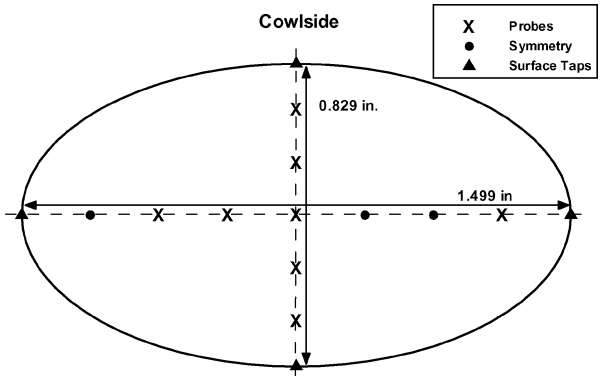

Fig. 4 Schematic of pitot-probe positions at the inlet exit.

prior to unstart. Figure 4 shows the positions of the pitot probes at the inlet exit. The vertical plane of symmetry and use of adjacent surface pressure taps enabled the exit flow to be mapped in some detail with only eight probes.

Inlet Geometry

The REST inlet model used in the test program was an improved version of that tested at Mach 6.2 (Ref. 7). Changes to the preceding shape were based on experience gained during the Mach 6.2 test program and the additional requirement for self-starting at Mach 4.0. These changes included the following: 1) A 20% reduction in inlet length (as a result of a less conservative boundary-layer separation criterion), 2) slight reduction of the design point from Mach 6.0 to Mach 5.7, and 3) cutback of the cowl to allow more flow spillage and a reduced internal contraction ratio.

Changes 2 and 3 were in response to the reduction of the self-starting requirement from Mach 6.2 to Mach 4.0. As discussed in Ref. 9, the key parameters for characterizing inlet starting are the internal contraction ratio and the Mach number at the plane of cowl closure, M_{close}. The lower the value of M_{close}, the more the internal contraction ratio must be reduced to allow self-starting. This trend applies to all inlet configurations, but the correlation between M_{close} and internal contraction ratio for particular inlet configurations is very geomtry specific, and can only be ascertained through experiment. In the absence of experimental data, the Kantrowitz starting limit[5] is usually used to determine the allowable internal contraction ratio for inlet starting.

The previous REST inlet self-started at Mach 6.2 with an internal contraction ratio of 2.15 and $M_{\text{close}} = 4.68$. This level of internal contraction is well above the Kantrowitz starting limit[5] of 1.53 at $M_{\text{close}} = 4.68$. The ability of the REST inlet configuration to self-start at internal contraction ratio's above the Kantrowitz limit was extrapolated to Mach 4.0, resulting in the current inlet configuration, which has an $M_{\text{close}} = 2.90$ (when operating at Mach 4.0) and an internal contraction ratio of 1.77. The Kantrowitz starting limit in this instance is 1.38. A significant amount of computational-fluid-dynamics (CFD)-based analysis was performed to ensure that this new REST inlet geometry retained the good on-design performance levels of the original configuration.

As already stated, the ability of current REST inlet to self-start at Mach 4.0 could only be confirmed by experiment. Because of the notoriously unpredictable nature of inlet start-ability, space was provided for the addition of "spill" holes on the sides and cowl of the inlet between cowl closure and the throat. When initial tests indicated that the current inlet would not self-start at Mach 4, numerous $\frac{1}{8}$-in.-diam holes directed at 45 deg to the downstream direction of the local surface were drilled in these areas. Figure 5 shows a close-up view of some of these holes, which were able to be filled and reopened as required. These holes constituted a passive system for spilling enough mass to allow the inlet to self-start. They also spilled at a reduced level once the inlet was started. This inlet starting technique has considerable system-level advantages over more elaborate methods involving variable geometry or active bodyside bleed systems.

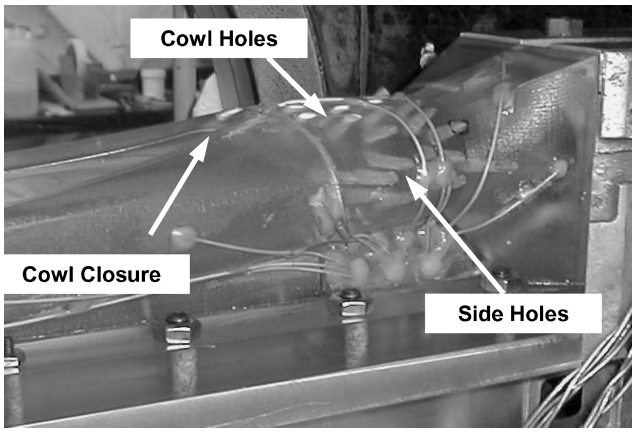

Fig. 5 Close-up view of inlet spillage holes.

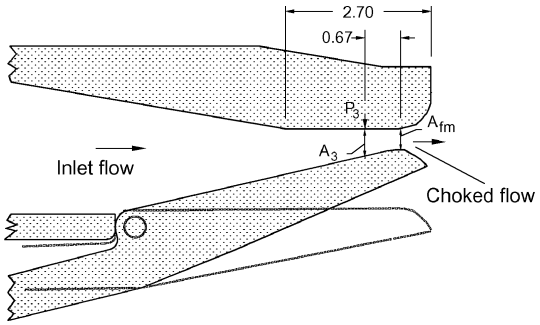

Fig. 6 Schematic of the rear section of the flowmeter.

Flow-Meter Operation

The flowmeter used for the current experiments was calibrated in the M4BDF for operation in the range of 0.75 to 1.60 lb/s. This device was installed directly downstream of the inlet (see Fig. 1) and consisted of a rectangular duct with a rotating rear flap for exit area adjustment. The flow rate of air captured by the inlet, $\dot{m}_{\text{cap}}$, was measured by reducing the exit area of the flowmeter to the point where flow was choked. The device was also used to apply back-pressure to the inlet. Figure 6 shows a schematic of the rear section of the flowmeter. The method used to measure $\dot{m}_{\text{cap}}$ utilized the static pressure measured a short distance upstream of the flowmeter exit (labeled station 3). The mass capture ratio of the inlet, m_c, is defined as

$$m_c = \dot{m}_{\text{cap}}/\dot{m}_{100\%} \tag{1}$$

Defining C_D as the discharge coefficient for the flowmeter and using subscript 1 to indicate wind-tunnel freestream conditions, it follows that

$$m_c = \frac{\rho_3 u_3 A_3 C_D}{\rho_1 u_1 A_{\text{cap}}} \tag{2}$$

The discharge coefficient was determined from calibration at freestream conditions and flow rates similar to the inlet tests to be $C_D = 0.999 \pm 0.002$. Assuming a calorically perfect gas and adiabatic flow through the inlet and flowmeter, the inlet capture ratio is given by

$$m_c = \frac{M_3 p_3 A_3 C_D}{M_1 p_1 A_{\text{cap}}} \sqrt{\frac{1 + [(\gamma - 1)/2]M_3^2}{1 + [(\gamma - 1)/2]M_1^2}} \tag{3}$$

The assumption of sonic flow at the throat of the flowmeter makes M_3 an implicit function of A_{fm} and A_3, as follows:

$$A_{\mathrm{fm}}/A_3 = [(\gamma+1)/2]^{(\gamma+1)/2(\gamma-1)} \times M_3\left\{1+[(\gamma-1)/2]M_3^2\right\}^{-(\gamma+1)/2(\gamma-1)} \quad (4)$$

The ratio A_{fm}/A_3 is a function of A_{fm}, which was measured using a potentiometer during each test. The Mach number at station 3 was then calculated from Eq. (4) and substituted into Eq. (3) along with other measured quantities to determine m_c. The uncertainty associated with mass capture ratio's calculated using this method was estimated to be $\pm 2.5\%$ using standard uncertainty analysis techniques.

Experimental Results

The goals of the experimental program were twofold: 1) to ascertain whether the as-designed inlet would self-start at Mach 4, and if not, how many spill holes would be needed for self-starting; and 2) to characterize the performance and backpressure limits of a REST inlet at Mach numbers well below the design point. Initial tests showed that the inlet did require spill holes in order to start at Mach 4.0. After considerable testing of different spillage configurations (varying the number, axial position, and circumferential position of holes), it was found that holes on the side of the inlet were most effective, and a minimum of 16 holes (eight on each side) were required for self-starting.

Characteristics of Self-Starting Inlet Configurations

Figure 7 shows the time history of the flowmeter throat area A_{fm}, the mass capture ratio m_c, and the symmetry plane pressure taps located inside (p_{in}) and outside (p_{out}) the cowl (just downstream of cowl closure). These particular data are for the self-starting configuration with 30 side holes. In this run the inlet started with the tunnel at $t = 0$ s with the flowmeter fully opened. As A_{fm} was gradually decreased, the inlet experienced an increasing backpressure level until unstart occurred at approximately $t = 86$ s. Unstart is indicated in Fig. 7 by an instantaneous drop in m_c and an accompanying change in both p_{in} and p_{out}. Subsequent increase of A_{fm} reduced the applied backpressure, and the inlet was observed to restart at approximately $t = 98$ s. Restart of an inlet after such a mechanically imposed unstart is proof of its ability to self-start at these inflow conditions. Note that the plotted value of m_c varies wildly until approximately $t = 20$ s, and subsequently approaches the correct level at approximately $t = 40$ s. This behavior occurs because the assumption of sonic flow at the throat of the flow meter is not valid until A_{fm} is reduced to some threshold value, in this case approximately 2.1 in.^{2}

Another feature of the inlet shown in Fig. 7 is the decrease in m_c observed prior to unstart. This particular configuration had a started mass capture ratio of $m_c = 0.763$. Just before unstart, however, m_c reduced to 0.715. As both p_{in} and p_{out} remained unchanged until inlet unstart, no preunstart spillage occurred in front of the cowl. The reduced mass capture was solely as a result of increased spillage through the starting holes as the backpressure level increased inside the inlet. The wall thermocouple measurements (not shown) indicated that the model reached adiabatic wall conditions early in the run and remained at this temperature throughout.

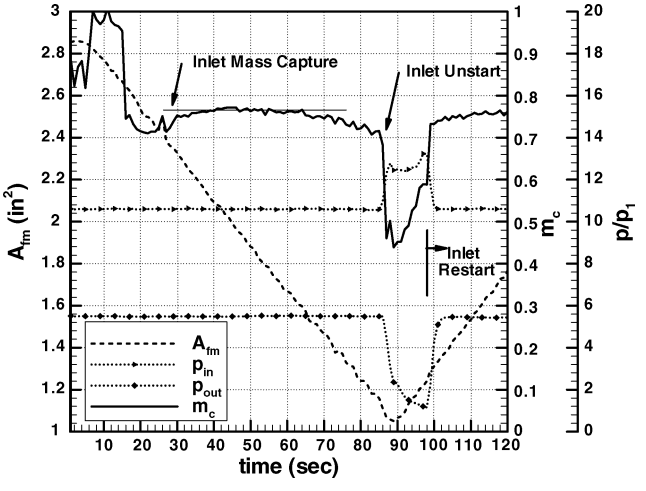

Fig. 7 Plot of key parameters during a run with the 30-side-hole configuration.

Fig. 8 Schlieren image of the started flowfield of the minimum spillage configuration.

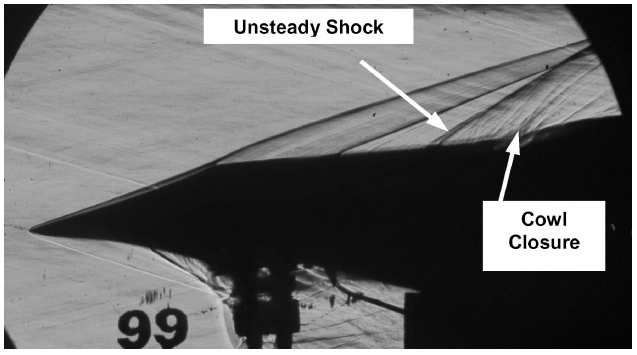

Fig. 9 Instantaneous schlieren image of the unstarted flowfield of the minimum spillage configuration.

Figure 8 shows a schlieren image of a typical test when the inlet was started. Flow is from left to right, and the steady external shock structure above the inlet contained initial waves from the leading edges of the inlet, a second wave emanating from the lower or bodyside leading edge, and finally the shock emanating from the point of cowl closure. Numerous other waves can be detected in the image, some of which are generated by the external pressure tubing. Figure 9 shows an instantaneous schlieren image of the unsteady flowfield that occurred after unstart. In this instance the cowl closure shock of the started flowfield is replaced by a shock of higher strength that oscillates slightly upstream of cowl closure. The remainder of the external shock structure appeared identical to that observed when the inlet was started (Fig. 8).

Figure 10 shows the normalized pressure distributions along instrumentation streamlines A, C, D, E, G, and H for the minimum spillage configuration (16 side holes) during tare operation, that is, with no backpressure. The pressure levels on each streamline increased gradually up to cowl closure, indicating that all surfaces are contributing to the compression. The internal flow downstream of cowl closure was dominated by the three-dimensional cowl shock that reflected multiple times before the inlet exit. The close correlation between the pressure distributions on streamlines D and H confirmed that the flow is nearly symmetric. The tare mass capture ratio for this minimum spillage configuration was $m_c = 0.797$, and the average compression ratio at the inlet exit was $p_{\mathrm{ex}}/p_1 = 12.60$.

The body-side pressure distributions (streamline A) for the minimum spillage configuration during tare operation, maximum backpressure, and after unstart are shown in Fig. 11. The tare pressure distribution shows gradual pressure rise upstream of cowl closure and the effect of cowl shock reflections downstream of cowl closure. The maximum backpressure plot displays upstream influence well beyond the inlet throat and a maximum backpressure ratio

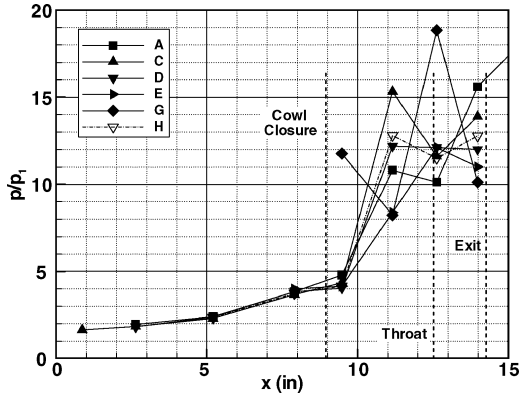

Fig. 10 Surface pressure distribution for tare operation.

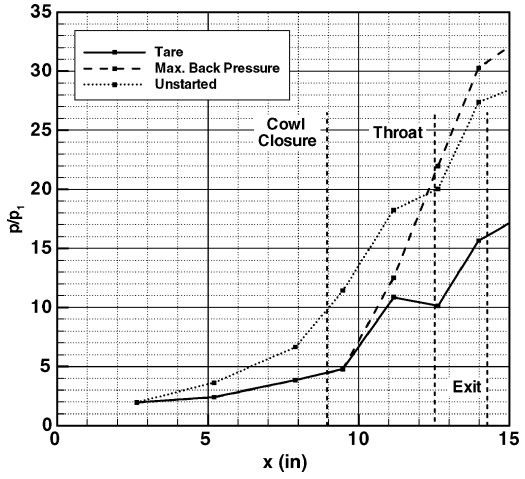

Fig. 11 Body-side pressure distributions at different stages of a test.

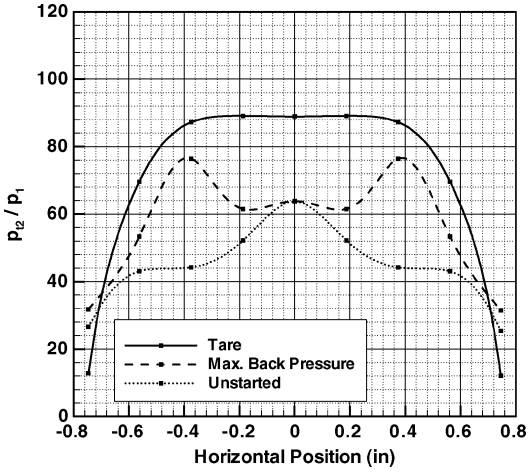

Fig. 12a Horizontal pitot distributions at the inlet exit.

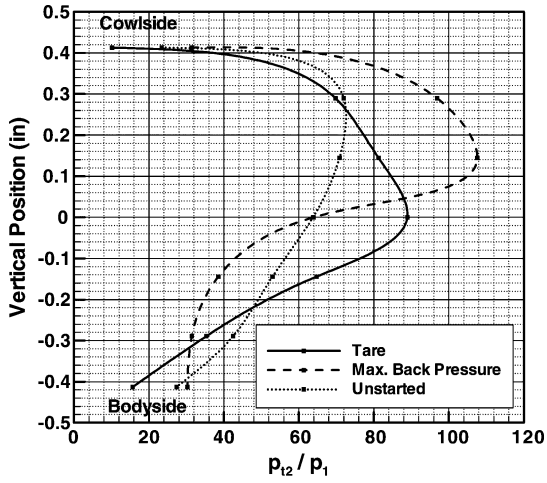

Fig. 12b Vertical pitot distributions at the inlet exit.

at the inlet exit of $p_{\max}/p_1 = 30.29$. This is a factor of 2.40 greater than the tare compression ratio for this configuration. The unstarted flowfield influenced all but the most forward body-side pressure tap and led to a reduction in mass capture ratio to $m_c = 0.59$. The unstarted plot also shows a backpressure level of $p_{\text{uns}}/p_1 = 27.5$ at the inlet exit, which is approximately 90% of the maximum backpressure. This form of "soft" unstart is more typical of inlets with considerably lower internal contraction ratios and is postulated to be caused by the presence of the spillage holes.

Figures 12a and 12b display the normalized pitot pressure distributions along horizontal and vertical branches of the pitot rake at the inlet exit, respectively. Included in the figures are the tare, maximum backpressure, and unstart distributions for the minimum spillage configuration. During tare operation, the horizontal pitot distribution (Fig. 12a) was constant through the core of the exit flow at a value of $p_{t2}/p_1 \sim 89$. At maximum backpressure the distribution included two lobes with a local maxima of $p_{t2}/p_1 \sim 77$ on either side of the central region, which dropped to a level of $p_{t2}/p_1 \sim 62$. This form of spanwise pitot distribution is caused by the presence of a shock train near the throat of the inlet; however, more inflow measurements would be required to supply a detailed physical explanation for the observed distribution. Once the inlet unstarted, the pitot pressure dropped by a considerable margin, except at the center of the span where it remained at the same level as at the maximum back-pressure condition.

The vertical pitot distribution (Fig. 12b) for tare operation peaked at the center of the inlet exit at $p_{t2}/p_1 \sim 89$. Pitot pressure remained at a high level on the cowl side of the span, while decreasing more quickly on the bodyside. This feature was also observed in the previous Mach 6 experiments.[7] At maximum backpressure the pitot distribution was significantly transformed. In this instance the flow separated into two distinct regions: 1) a cowl-side region with high pitot levels that peaked at $p_{t2}/p_1 \sim 108$ (well above the maximum observed during tare operation) and 2) a body-side region, which had very low pitot levels not much greater than the body-side wall pressure. This type of pitot distribution is consistent with computational solutions of the backpressured Mach 6 REST inlet that were reported in Ref. 8. These solutions indicated a flowfield containing an asymmetric shock train on the cowl side of the inlet, with highly distorted flow adjacent to the bodyside. The vertical pitot distribution for the unstarted flow showed highest levels on the cowl side, reaching a maximum of $p_{t2}/p_1 \sim 72$ near the cowl.

Self-starting configurations with up to 40 spill holes (20 on the cowl; 10 on each side) were tested in the program. Mass capture values varied between $m_c = 0.758$ for the 40-hole configuration to $m_c = 0.797$ for the minimum spillage configuration with 16 holes (eight on each side). The inlet compression ratio, determined from the average of the eight surface pressure taps at the exit of the inlet during tare operation, ranged between $p_{\text{ex}}/p_1 = 11.7$ and 13.5 for all configurations. The maximum backpressure ratio, determined from the average of the exit pressure taps at the point of maximum backpressure, remained relatively constant for all configurations, varying between $p_{\max}/p_1 = 29.8$ and 31.5. These inlet performance parameters compare favorably with those obtained from testing of a two-dimensional, variable geometry hypersonic inlet configuration operating at Mach 4.0 with similar L_{isol}/D_h (Ref. 10). These test results supply some measure of confidence in the ability of REST inlet configurations to operate effectively at conditions well below the design point.

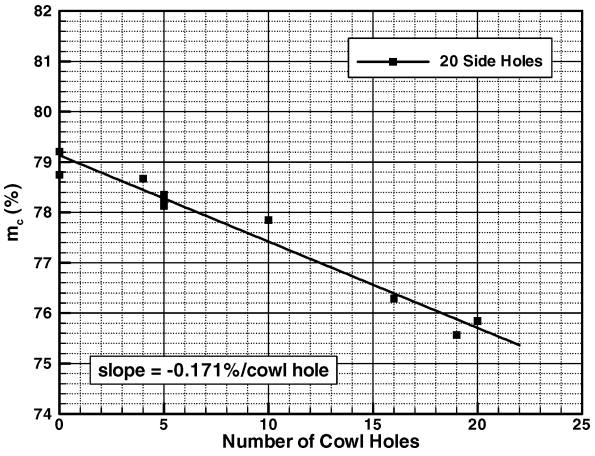

Fig. 13a Started mass capture variation with number of cowl holes.

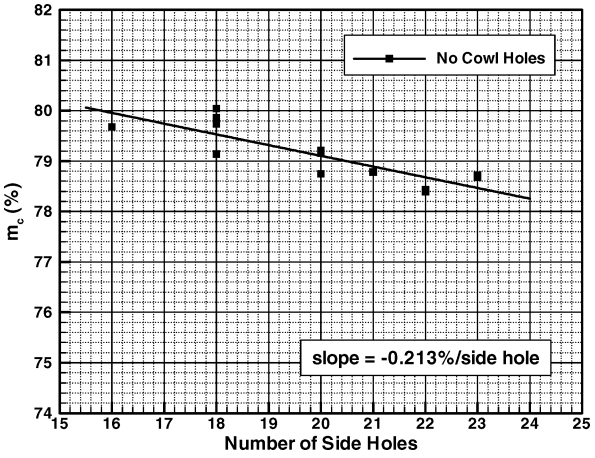

Fig. 13b Started mass capture variation with number of side holes.

Effect of Spillage Hole on Started Mass Capture

As the test program progressed, it became clear that spillage holes on the cowl were far less effective than spillage holes on the side for improving inlet start ability. For example, a configuration with 16 side holes was found to self-start, but a configuration with 10 side holes and 20 cowl holes would not. In this case an extra six side holes moved the inlet more towards self-starting than the addition of 20 cowl holes. It is postulated that this difference is caused by the thicker boundary layer on the sides of the inlet relative to the boundary layer on the cowl. The greater the proportion of boundary-layer fluid that is spilled, the higher is the average total pressure of the remainder of the air that must pass through the inlet throat, and the more effective the spillage is in improving start ability. The greater thickness of the side-wall boundary layer (relative to the thickness of the cowl boundary layer) is expected to lead to a higher proportion of boundary-layer spillage through side holes and greater effectiveness of side holes for improving start ability.

The holes continued to spill after the inlet configuration was started, albeit at a reduced level. The started spillage losses of both the side and cowl holes were quantified by examining two separate groupings of the data: 1) with the number of side holes constant and 2) with the number of cowl holes constant. Figure 13a shows a plot of started inlet mass capture vs the number of cowl holes present, for all configurations with 20 side holes. The data show a relatively linear decrease in m_c with the addition of more cowl holes, and a linear fit to the data indicates a reduction of 0.171% in m_c for each cowl hole. Figure 13b shows a plot of started m_c vs the number of side holes present for all configurations with no cowl holes. A linear fit to this data indicated a reduction of 0.213% in m_c for each side hole. Based on this level of spillage, the minimum penalty for enabling the current inlet configuration to self-start is a 3.4% reduction in the mass capture of the inlet.

Conclusions

Results of Mach 4.0 wind-tunnel testing of a fixed-geometry hypersonic inlet were reported. The tested quasi-streamline-traced inlet had a geometric contraction ratio of 4.80, an internal contraction ratio of 1.77, and a Mach 5.7 design point. It also included a transition from a nearly rectangular capture to an elliptical throat and an elliptical isolator with $L_{\text{isol}}/D_h = 1.68$. The tests were conducted to determine the performance and starting limits of the inlet at a Mach number well below the design point.

Initial testing of the inlet indicated that it would not self-start at Mach 4.0. This limitation was overcome by the introduction of $\frac{1}{8}$ in. diam spillage holes on the cowl or sides of the inlet between cowl closure and the inlet throat. Numerous spillage hole configurations were examined during the test program, and it was observed that holes on the sides of the inlet were more effective than holes on the cowl for improving inlet start ability. It was postulated that this was caused by side holes spilling a larger proportion of boundary-layer fluid than cowl holes. The self-starting configuration with minimum spillage included a total of 16 holes, eight on each side of the inlet. Once started, this configuration generated a compression ratio of 12.6, captured 79.7% of the available air, and withstood a mechanically imposed backpressure ratio of 30.3 relative to the tunnel static pressure. The started spillage loss caused by the presence of the holes was estimated to be 3.4% of the available air.

These experiments show that good performance is obtainable from streamline-traced inlet configurations at Mach numbers well below the design point. In conjunction with the previous experiments at on-design conditions,[7] the current results indicate that fixed-geometry inlets with rectangular-to-elliptical shape transition are a viable configuration for airframe-integrated scramjets that operate over a significant Mach-number range.

Acknowledgment

The first author wishes to thank Mark Cagle of the Model Systems Branch at NASA Langley Research Center for his help with the design and fabrication of the model, and NASA technician Fred Rudolph for operation of the wind tunnel.

References

[1]Hartill, W. B., "Analytical and Experimental Investigation of a Scramjet Inlet of Quadriform Shape," U.S. Air Force, Tech. Rept. AFAPL-TR-65-74, Aug. 1965.

[2]Billig, F. S., "Supersonic Combustion Ramjet Missile," *Journal of Propulsion and Power*, Vol. 11, No. 6, 1995, pp. 1139–1146.

[3]Kutshenreuter, P. H., "Hypersonic Inlet Tests in Helium and Air," Dept. of Advanced Engine and Technology, General Electric Co., Cincinnati, OH, June 1965.

[4]Molder, S., and Romeskie, J. M., "Modular Hypersonic Inlets with Conical Flow," *AGARD Conference Proceedings*, No. 30, 1968.

[5]Kantrowitz, A., and Donaldson, C., "Preliminary Investigation of Supersonic Diffusers," NACA WR L-713, 1945.

[6]Smart, M. K., "Design of Three-Dimensional Hypersonic Inlets with Rectangular-to-Elliptical Shape Transition," *Journal of Propulsion and Power*, Vol. 15, No. 3, 1999, pp. 408–416.

[7]Smart, M. K., "Experimental Testing of a Hypersonic Inlet with Rectangular-to-Elliptical Shape Transition," *Journal of Propulsion and Power*, Vol. 17, No. 2, 2001, pp. 276–283.

[8]Smart, M. K., and White, J. A., "Computational Investigation of the Performance and Back-Pressure Limits of a Hypersonic Inlet," AIAA paper 2002-0508, Jan. 2002.

[9]Van Wie, D. M., Kwok, F. T., and Walsh, R. F., "Starting Characteristics of Supersonic Inlets," AIAA Paper 96-2914, July 1996.

[10]Emami, S., Trexler, C. A., Auslender, A. H., and Wiedner, J. P., "Experimental Investigation of Inlet-Combustor Isolators for Dual-Mode Scramjet at a Mach Number of 4," NASA TP 3502, May 1995.